Materials Today Bio 18 (2023) 100536

Contents lists available at ScienceDirect

Materials Today Bio

journal homepage: www.journals.elsevier.com/materials-today-bio

Micropatterned photothermal double-layer periosteum with angiogenesis-neurogenesis coupling effect for bone regeneration

Qing Li [a,1], Wenbin Liu [d,1], Wen Hou [a], Xiaopei Wu [a], Wenying Wei [a], Jiawei Liu [a], Yihe Hu [c,**], Honglian Dai [a,b,*]

[a] State Key Laboratory of Advanced Technology for Materials Synthesis and Processing, Biomedical Materials and Engineering Research Center of Hubei Province, Wuhan University of Technology, Wuhan, 430070, China
[b] Shenzhen Institute of Wuhan University of Technology, Shenzhen, 518000, China
[c] Department of Orthopedic Surgery, The First Affiliated Hospital, College of Medicine, Zhejiang University, Hangzhou, 310003, China
[d] Department of Orthopaedics, The Third Xiangya Hospital, Central South University, 138 Tongzipo Road, Changsha, 410008, China

ARTICLE INFO

Keywords:
Biomimetic periosteum
Neurovascularization
Surface micropatterns
Osteogenesis
Electrospinning

ABSTRACT

The abundant neurovascular network in the periosteal fibrous layer is essential for regulating bone homeostasis and repairing bone defects. However, the majority of the current studies only focus on the structure or function, and most of them merely involve osteogenesis and angiogenesis, lacking an in-depth study of periosteal neurogenesis. In this study, a photothermal double-layer biomimetic periosteum with neurovascular coupling was proposed. The outer layer of biomimetic periosteum is a conventional electrospinning membrane to prevent soft tissue invasion, and the inner layer is an oriented nanofiber membrane to promote cell recruitment and angiogenesis. From the perspective of functional bionics, based on the whitlockite (WH) similar to bone composition, we doped Nd (the trivalent form of neodymium element) in it as the inducing element of photothermal response to prepare photothermal whitlockite (Nd@WH). The sustained release of Mg^{2+} in Nd@WH can effectively promote the up-regulation of nerve growth factor (NGF) and vascular endothelial growth factor (VEGF). The release of Ca^{2+} and PO_4^{3-} ions and photothermal osteogenesis jointly promote bone regeneration. Under the combined effect of structure and function, the formation of nerves, blood vessels, and related collagens greatly simulates the microenvironment of extracellular matrix and periosteum regeneration and ultimately promotes bone regeneration. In this study, physical and chemical characterization proved that the bionic periosteum has good flexibility and operability. The *in vitro* cell experiment and *in vivo* calvarial defect model verified that PPCL/Nd@WH biomimetic periosteum had excellent bone tissue regeneration function compared with other groups. Finally, PPCL/Nd@WH provides a new idea for the design of bionic periosteum.

1. Introduction

The bone defect caused by trauma and disease is still a major challenge in orthopedics. The design of traditional bone repair materials mostly ignores the importance of the periosteum for bone integrity and bone regeneration, especially during fracture repair. Studies have shown that the primary task is the reconstruction of the periosteum [1]. As the understanding of bone tissue repair becomes more advanced, periosteum reconstruction has gradually become one of the research hotspots. The native periosteum is a thin and tough connective tissue surrounding the bone tissue, which not only has an osteogenic but also has an osteoclastic role in bone homeostasis. The periosteum generally has two layers of structure, the inner cell layer, and the outer fiber layer. The inner cell layer contains osteoblasts and mesenchymal stem cells. The outer fiber layer has abundant neurovascular associated networks and collagen fibers, which can provide nutrients and signaling molecules for bone tissue and maintain bone homeostasis [2,3]. The ideal bionic periosteum should have the functions of flexibility, barrier function, and imitation of the periosteum microenvironment.

Based on the two-layer structure of the natural periosteum, many

* Corresponding author. State Key Laboratory of Advanced Technology for Materials Synthesis and Processing, Wuhan University of Technology, Wuhan, 430070, China.
** Corresponding author.
E-mail addresses: xy_huyh@163.com (Y. Hu), daihonglian@whut.edu.cn (H. Dai).
[1] These authors contributed equally to this work.

https://doi.org/10.1016/j.mtbio.2022.100536
Received 17 September 2022; Received in revised form 4 December 2022; Accepted 27 December 2022
Available online 28 December 2022

researchers give inspiration from structural bionics. Recent studies have shown that orientation nanofibers can mimic the topological clues of fibronectin to accurately control cell alignment and phenotypic expression. In particular, silk fibroin nanofibers scaffolds simulating extracellular matrix structure can not only induce the directional growth of neurons but also derivate the growth, migration, and arrangement of endothelial cells [4–10]. Yang et al. verified that rat mesenchymal stem cells showed highly arranged tissues on the material through a micropattern design of the surface-oriented structure, which eventually led to enhanced angiogenesis and osteogenic expression [11]. Zhang et al. proved that the way BMSCs (Bone marrow-derived mesenchymal stem cells) deposited collagen and minerals on PCL substrate with micro patterns on oriented structure surface was highly similar to that of natural bone extracellular matrix [12]. The construction of biomimetic periosteum with oriented micropatterns may promote the differentiation of cells in the defect area into osteoblasts and may promote angiogenesis. Therefore, it is not difficult to find that material design with a surface-oriented structure can promote neurogenesis, angiogenesis, and osteogenesis. Therefore, this excellent structure introduced into the design of the bionic periosteum can promote the reconstruction of the periosteum microenvironment in the bone defect.

Besides structural bionic design. functional bionics is also important in periosteum reconstruction and bone repair. In recent years, more and more researchers have confirmed that the periosteum plays an important role in bone repair [1,13–15]. At present, most researchers focus on the important effect of vascular regeneration on bone repair, ignoring the important role of nerves in bone repair [16–19]. WH is the second-highest mineral in human bone. Some studies have shown that WH can reproduce early bone regeneration by increasing the ion concentrations of Ca^{2+} and PO_4^{3-} and inhibiting the differentiation of osteoclasts [20,21]. At the same time, the sustained release of Mg^{2+} in WH was proved to promote the secretion of NGF and VEGF [22–25]. WH has potential as an active substance of neuroangiogenesis and bone formation in biomimetic periosteum to reconstruct the periosteum microenvironment at the defect site.

Photothermal physical stimulation has been widely used in the field of bone repair in recent years. Near-infrared irradiation can give appropriate thermal stimulation (40 ± 0.5 °C) to the defect site to promote bone repair [26–28]. Nd, as an element with photothermal response characteristics, has gradually attracted people's attention. For this purpose, Nd was doped into WH, and a new type of Nd @ WH was first developed by hydrothermal synthesis. Based on maintaining the original Ca^{2+}, Mg^{2+}, and PO_4^{3-} ions, the photothermal response performance of WH was given. It not only maintains the original osteogenesis performance but also endows the photothermal response of nanoparticles with osteogenesis characteristics to achieve the superposition of osteogenesis effects.

In this study, based on the structural and functional properties of natural periosteum, a double-layer PCL (Polycaprolactone) nanofiber membrane with a surface-oriented structure, and loaded with Nd@WH nanoparticles was developed by combining electrospinning technology with laser etching technology (Fig. 1). It is denoted as PPCL/Nd@WH. Firstly, The template with a surface-oriented structure was prepared by laser etching technique for collecting electrospinning membrane. The micropattern of the inner layer-oriented structure of the bionic periosteum not only provides space for the regular close arrangement of cells in the body but also provides a specific surface structure for bone formation and angiogenesis. The outer layer of the bionic periosteum is a conventional electrospinning membrane, which can effectively inhibit the invasion of soft tissue to bone tissue. In addition, in terms of function, Ca^{2+} and PO_4^{3-} in Nd@WH can promote early bone regeneration, and continuously released Mg^{2+} can effectively promote the regeneration of nerves and blood vessels. At the same time, photothermal osteogenesis and ionic interaction together promote bone regeneration in the defect site. Finally, we proved that the bionic periosteum has good flexibility and operability by physical and chemical characterization. *In vitro* cell experiment and *in vivo* skull defect model verified that PPCL/Nd@WH biomimetic periosteum had excellent osteoinductive properties and can enhanced early vascularization and neurogenesis, which prompted eventual bone regeneration and remodling. Finally, the proposed strategy for the development of PPCL/Nd@WH biomimetic periosteum provides new insights into the design of biological materials.

2. Materials and methods

2.1. Materials

PCL (Mw = 8000 Da) was purchased from Sigma. Hexafluorin isopropanol solvent was obtained from Aladdin. WH and Nd@WH nanoparticles were synthesized by precipitation method according to a certain proportion of calcium hydroxide, magnesium hydroxide, phosphoric acid, and neodymium oxide in a water-based system. (all materials were purchased from Sinopharm Chemical Reagent Co., Ltd. (China) and were used as received without further purification). The fetal bovine serum (FBS) was purchased from Procell Life Science &Technology Co., Ltd. (China). The CELLSAVING was purchased from NCM Biotech (C40100, Suzhou, China). The Glass Bottom Cell Culture Dish for confocal microscope photography was purchased from SORFA Life Science (China). The 250 ml culture medium bottles were purchased from Guangzhou Jet Bio-Filtration Co. Ltd. (China). The FITC-phalloidin and 4'6 diamidino-2-phenvlindole (DAPI) were purchased from Beijing Solarbio Science & Technology Co., Ltd. The transwell inserts of 24-well plates was purchased from NEST Biotechnology (725301, Wuxi, China). The SPARKscript II RT Plus kit (With gDNA Eraser) and 2 × SYBR Green qPCR Mix (with ROX) were purchased from the (Shandong Sparkjade Biotechnology Co., Ltd. (China). The NGF antibody was purchased from AiFang Biological (SAF005).

2.2. Preparation of different electrospun membranes

2.2.1. Preparation of conventional electrospinning film

The procedure of electrospinning method was performed according to our previously proposed preparation method. In brief, the electrospinning solution was added to a syringe (10 mL) with the NO.20 needle. Needle end and DC positive high voltage power supply connected with metal clips (Electrostatic spinning machine model SS-2535H). At the distance (15 cm) from the needle, the roller connecting DC negative high voltage power supply is placed. Finally, the syringe containing the spinning solution was placed on the injection pump of the spinning machine, and the electrospinning nanofibers were collected by the drum.

Three kinds of fibrous membranes, PCL, PCL/WH, and PCL/Nd@WH, can be collected from this collecting drum. For the PCL spinning solution, PCL was dissolved in hexafluoroisopropanol to prepare a 10% w w^{-1} spinning solution. For PCL/WH mixed solution, the synthesized WH was first dispersed in hexafluoroisopropanol, and then PCL was added to prepare the PCL/WH solution, where the weight ratio of PCL to WH was 1:1.5. Similarly, PCL/Nd@WH spinning solution with the same proportion was prepared. Three spinning solutions were collected according to specific parameters. Electrospinning parameters are flow rate 0.08 mm min^{-1}, positive voltage 5 kV, negative voltage 2 kV, collection distance 15 cm, and drum collection speed 100 rpm min^{-1}.

2.2.2. Preparation of surface micropatterned nanofiber membrane

Different from conventional electrospinning, for PPCL/Nd@WH nanofiber membrane, the nanofibers were collected using the template with surface aligned structure. The groove width, ridge width and groove depth of the orientation template collector were 100 μm, 100 μm, and 100 μm, respectively (RGD100). The spinning solution and spinning parameters were consistent with PCL/Nd@WH spinning membrane.

All electrospinning nanofiber membranes were vacuum dried overnight before use to completely remove residual solvents.

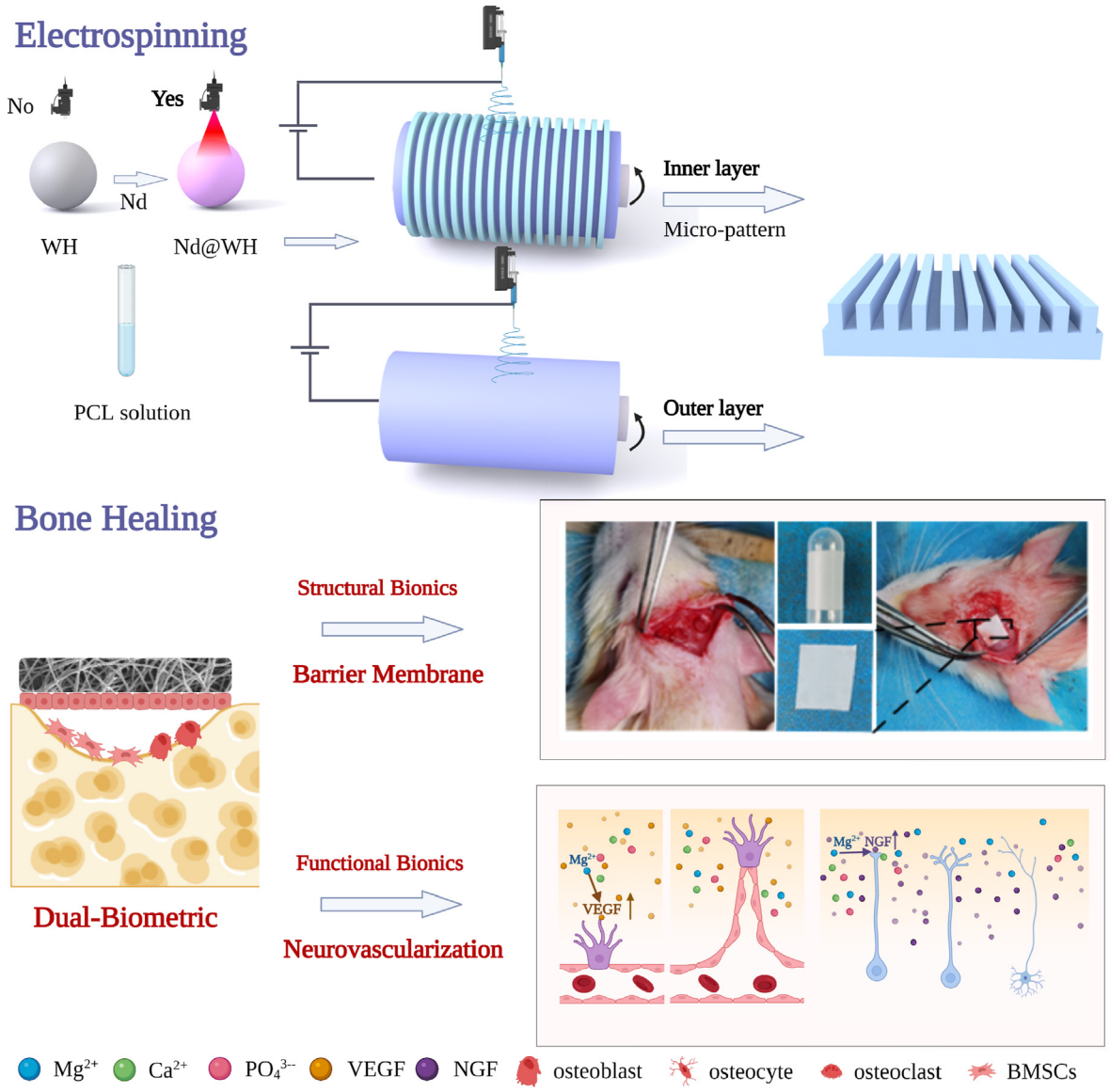

Fig. 1. Construction and repair process of photothermal double-layer biomimetic periosteum.

2.2.3. Characteristics of nanoparticles and membranes

the X-ray diffraction (XRD) and scanning electron microscopy (SEM) were used to verify the successful preparation of Nd@WH nanoparticles. The physical and chemical properties of different nanofiber membranes were tested by SEM, XRD, energy dispersive X-ray spectroscopy (EDS), tensile properties, photothermal response properties, and inductively coupled plasma optical emission spectroscopy (ICP-OES). The detailed procedures are shown in SI.

2.3. In vitro characterization of osteogenic experiment

Immunofluorescence and CCK-8 were used to verify the biocompatibility of cells on materials. The osteogenic differentiation ability of the cells was verified by Sirius red staining, Alizarin red staining, and Real-Time PCR analysis. The functional characterization of neurovascular was performed by migration assay and qPCR analysis. The detailed procedures are shown in SI.

2.4. In vivo regeneration of neurovascular and bone

Firstly, the angiogenesis effect of different nanofiber membranes *in vivo* was verified by a subcutaneous animal model. Secondly, immunofluorescence staining of nerve and blood vessels with specific markers NGF and CD31 was used to verify the regeneration of nerve and blood vessels in the rat skull defect model. Finally, in the rat skull defect model, Microcomputed Tomography Analysis and histological staining were used to verify the bone regeneration at the defect site. The detailed procedures are shown in SI.

2.5. Statistical analysis

The data were analyzed by GraphPad Prism 9. All data are expressed as mean ± standard deviation (SD). one-way analysis of variance (ANOVA) was used to test the differences among groups. The student's t-test was used to assess statistically significant differences in the data

between groups. Values of $P < 0.05$ were considered statistically significant.

3. Result

3.1. Characterization of nanofibers membrane

Firstly, as Confirmed by XRD and SEM, Nd@WH was successfully synthesized by the hydrothermal method (Fig. S1). In this study, as shown in Fig. 1, PCL nanofiber membranes were collected by a template collector, and one-step fabrication of micropatterned nanofiber membranes was denoted as PPCL. The SEM images confirmed the successful patterning of the nanofiber membranes. The micropattern size is RGD100 (Fig. 2A). PCL, PCL/WH, PCL/Nd@WH, and PPCL/Nd@WH nanofiber membranes were prepared according to the materials. Their surface morphology was observed by SEM. SEM images show that the 3D porous network is formed by nanofibers with a uniform diameter (Fig. 2B). The diameter was measured by Image-J software, and the average diameters of PCL, PCL/WH, PCL/Nd@WH, and PPCL/Nd@WH were 1060.91 ± 79.18 nm, 1333.79 ± 378.86 nm, 1124.50 ± 235.44 nm, and 1212.52 ± 305.83 nm, respectively (Fig. 2B). The three-dimensional morphology of all groups was obtained using micrographs of the three-dimensional surface morphology to simulate all groups. Based on this, the porous structure of the fiber membrane was observed (Fig. 2C).

EDS (Fig. 3D and Fig. S2) was used to determine the chemical composition and element distribution uniformity of the fiber membrane. According to the element distribution, the observation results showed that WH and Nd@WH nanoparticles were uniformly distributed in the fibers. Meanwhile, photothermal characteristic element Nd was detected in PCL/Nd@WH nanofilm.

XRD was used to further verify the chemical composition of PCL/WH and PCL/Nd@WH nanofiber membranes. For PCL, PCL/WH, and PCL/Nd@WH diffraction curves, the characteristics are 2θ: 21.40° and 23.86°, 2θ: 28.12°, 31.65°, and 35.24°, 2θ: 27.85°, 31.57°, 33.25° (Fig. 3A). These peaks were observed in the XRD patterns of different nanofiber membranes. The results showed that nanoparticles WH and Nd@WH were successfully incorporated into PCL fibers. The hydrophilicity of the fiber membrane was evaluated by testing the water contact angle. The water contact angles of PCL, PCL/WH, PCL/Nd@WH, and PPCL/Nd@WH were 144.20° ± 0.37°, 136.30° ± 0.99°, 135.80° ± 6.4°, and 135.93° ± 2.52°, respectively. On the fiber membrane containing nanoparticles, the water contact angle may decrease slightly compared with PCL due to the release of Ca^{2+} (Fig. 3C). The mechanical properties of nanofiber membranes were determined by a tensile strength test (Fig. 3B and Figs. S3–S5). The tensile stresses of PCL, PCL/WH, PCL/Nd@WH, and PPCL/Nd@WH were 4.97 ± 0.67 MPa, 0.76 ± 0.16 MPa, 0.86 ± 0.22 MPa, and 0.91 ± 0.09 MPa, respectively. The Young's modulus is 0.007 ± 0.0009 MPa, 0.003 ± 0.0002 MPa, 0.002 ± 0.0004 MPa, and 0.002 ± 0.0001 MPa, respectively. The tensile stress and Young's modulus show similar trends. The fracture strain of PCL showed the maximum value (733.32 ± 51.43%). PCL/Nd@WH and PPCL/Nd@WH exhibited similar fracture strains. According to the mechanical test, the nanofibers with two kinds of nanoparticles had similar mechanical properties, which were lower than those of PCL.

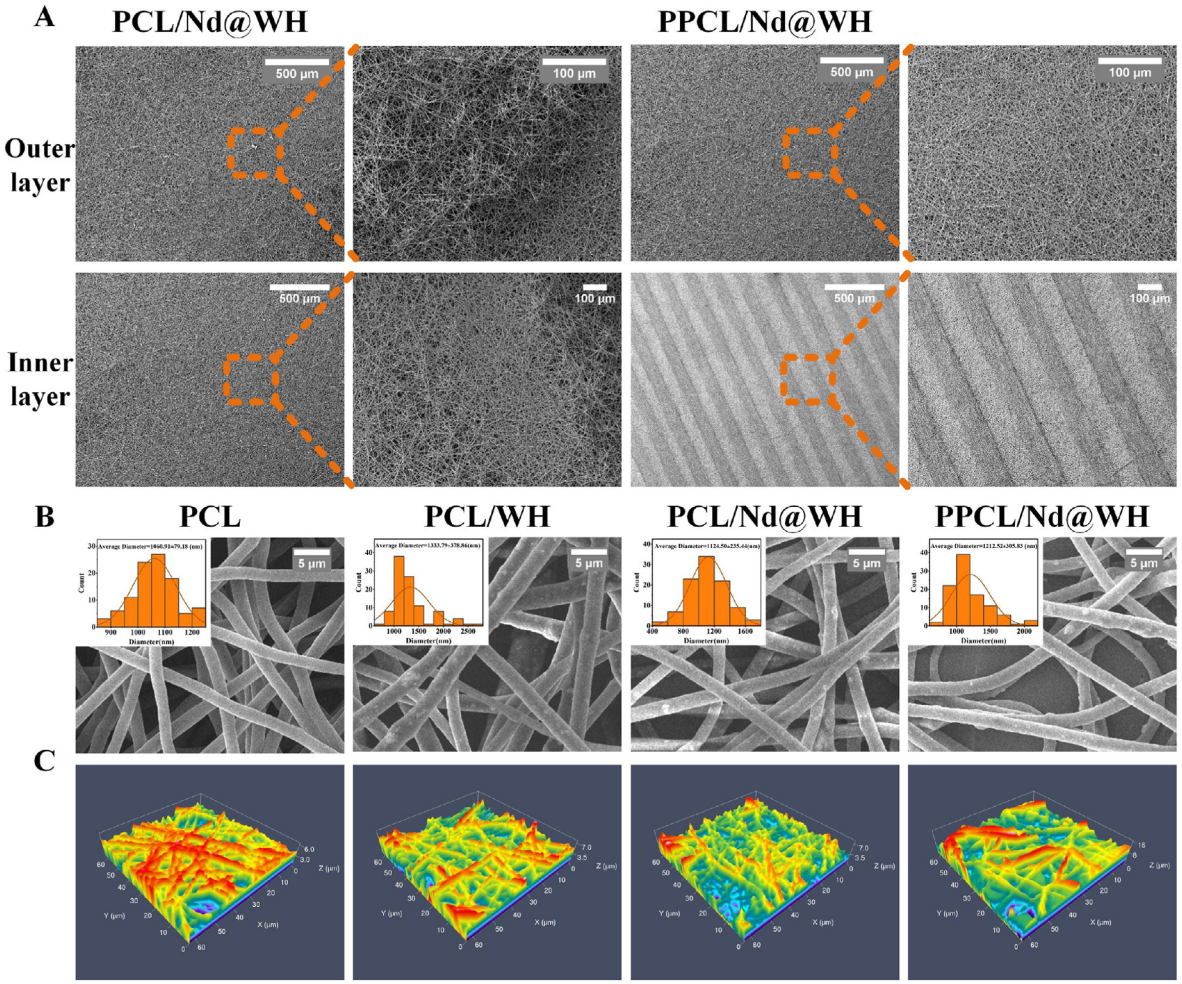

Fig. 2. Morphology characterization of the membrane. (A) (B) SEM micrographs; (C) 3D surface morphology microphotographs.

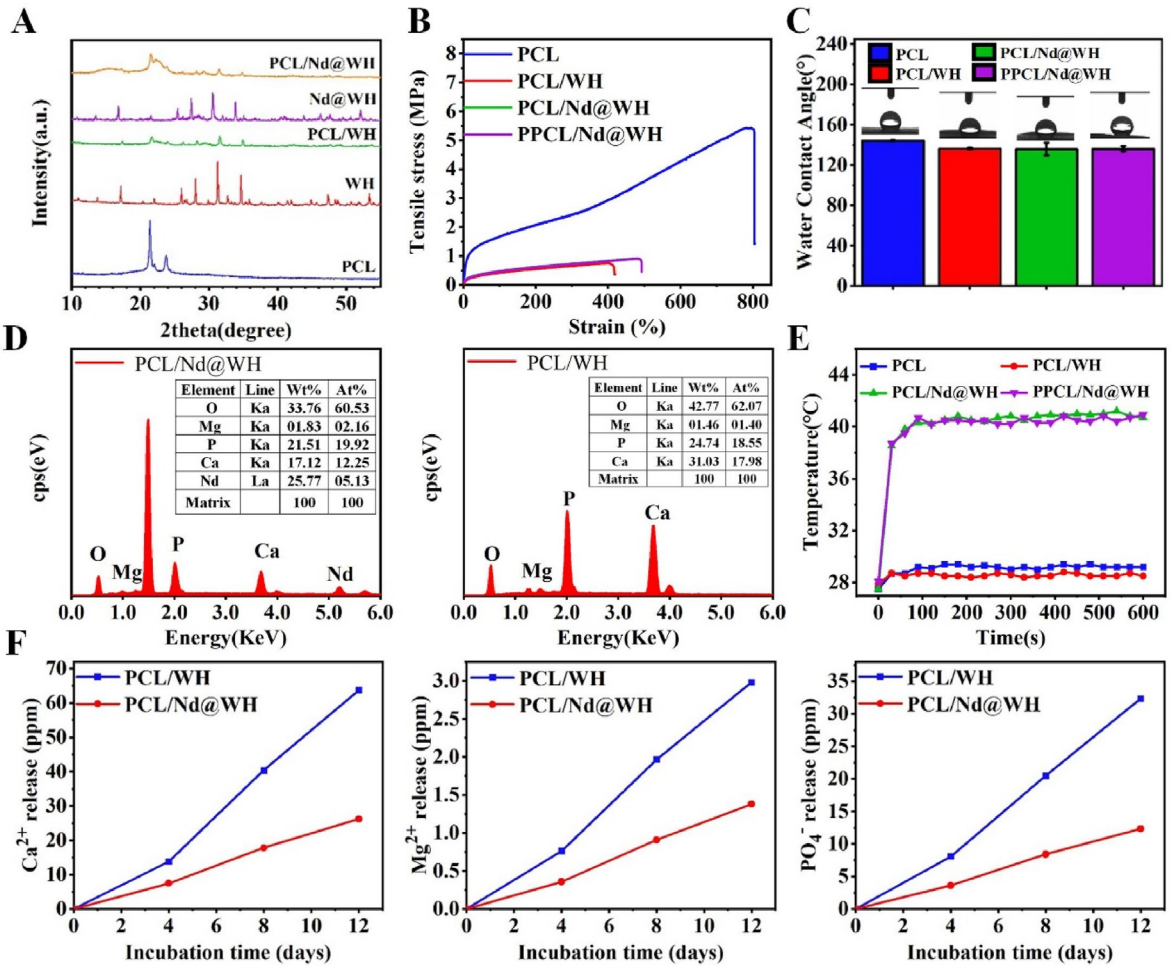

Fig. 3. (A) XRD diffraction of WH and Nd@WH nanoparticles and different nanofiber membranes. (B) stress-strain curve. (C) water contact angle. (D) elemental analysis microphotographs. (E) photothermal heating curves. (F) Ion release of Ca^{2+}, $Mg^{2+,}$ and PO_4^{3-}.

To determine the ion release behavior of the two nanoparticles, we measured the ion release characteristics of different nanocomposite films in the Tris-HCL buffer medium by inductively coupled plasma emission spectroscopy (Fig. 3F). The cumulative release curve showed that the release amount of Ca^{2+}, $Mg^{2+,}$ and PO_4^{3-} in WH was 2–3 times that of Nd@WH. And with the extension of time, the release amount of each ion showed an upward trend. In terms of this experiment, the release amount reached the highest at 12 days, but due to the additional amount being fixed, it is predicted that the ion release will reach equilibrium after a certain time point in the future. The release amounts of Ca^{2+}, $Mg^{2+,}$ and PO_4^{3-} in WH were 63.71 ppm, 2.98 ppm, and 32.35 ppm, respectively. The release amounts of Ca^{2+}, $Mg^{2+,}$ and PO_4^{3-} in Nd@WH were 26.20 ppm, 1.38 ppm, and 12.32 ppm, respectively.

The biodegradability of all nanofiber membranes was studied by incubation in PBS solution at 37 °C for 12 weeks. Through the study of PH degradation (Fig. S6), it was found that all fiber membranes showed degradation acidity. It could be observed that the degradation acidity of PCL/WH was greater than that of PCL/Nd@WH, indicating that PCL/Nd@WH implantation *in vivo* had a smaller impact on local pH. The degradation experiment (Fig. S7) showed that the weight loss rate of PCL fiber membrane reached 5.17 ± 0.82% after 12 weeks. The weight loss rate of PCL/WH was the highest after 12 weeks, reaching 18.66 ± 0.52%. PCL/Nd@WH and PPCL/Nd@WH showed similar degradation results, ranging from 8.8% to 8.9%. The results of weight loss show that the incorporation of nanoparticles can significantly improve the degradation effect of nanofiber membranes.

In terms of photothermal conversion mechanism, Nd rapidly relaxes to metastable state by radiationless process under 808 nm near-infrared excitation. Radiation is attenuated to a lower energy state in the metastable state, and phonon-assisted attenuation occurs in the ground state, resulting in photothermal conversion and heat generation. Then in order to verify the photothermal properties of PPCL/Nd@WH nanofiber membranes. The temperature change of the nanofiber membrane under 808 nm NIR irradiation (0.5 W/cm2) was recorded by the UNi260B infrared thermal imager (Fig. 4). Nanofiber membranes were irradiated with different irradiation powers, and the heating equilibrium temperature was recorded. At the power of 0.6 W/cm^2, the temperature finally stabilized at about 42 °C, higher than the required temperature for osteogenesis (40.5 ± 0.5 °C). At the power of 0.5 W/cm^2, the temperature is stable at about 40 °C, which meets the temperature required for osteogenesis. Therefore, 0.5 W/cm^2 power was selected for subsequent experiments (Fig. 4B).

However, the temperature of PCL and PCL/WH nanofiber membranes did not change significantly under the same NIR irradiation. The results of the photothermal heating curve show that the fiber membrane containing Nd@WH nanoparticles can reach the temperature balance after 100 s, and the temperature remains at the temperature required for osteogenesis (Fig. 3E). After that, PPCL/Nd@WH nanofiber membrane showed no significant difference in photothermal properties before and after irradiation during the five open/close cycles, indicating that the nanofiber membrane had excellent photothermal properties (Fig. 4C).

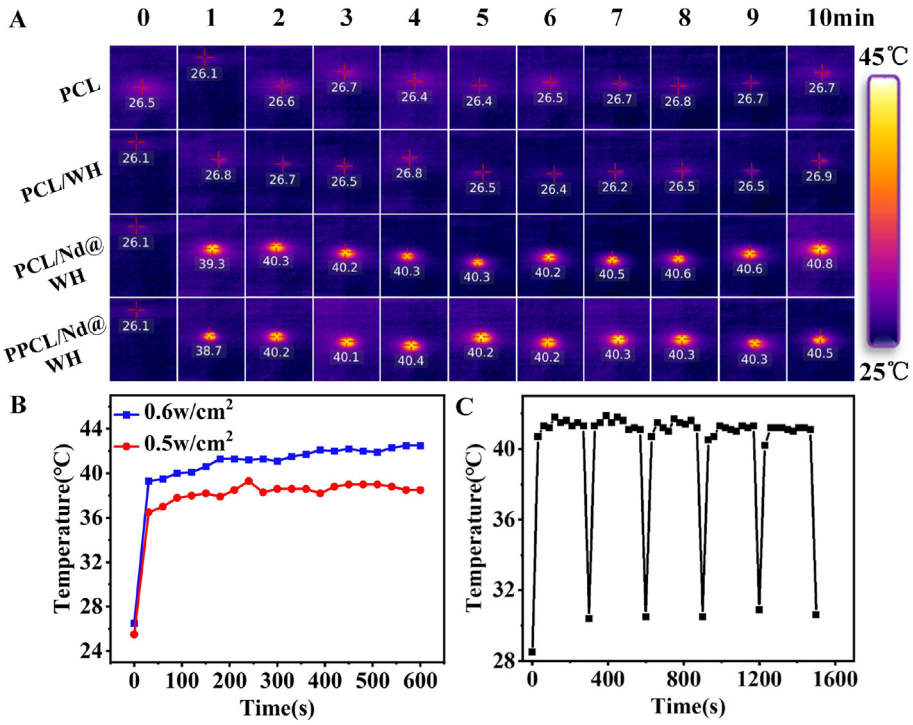

Fig. 4. (A) Infrared thermal imaging maps of different nanofiber membranes with the highest temperature symbol in the irradiation region. (B) Photothermal heating curve of membrane irradiated by 808 nm laser (0.6 W/cm^2 0.5 W/cm^2). (C) Temperature change of PPCL/Nd@WH during five ON/OFF cycles.

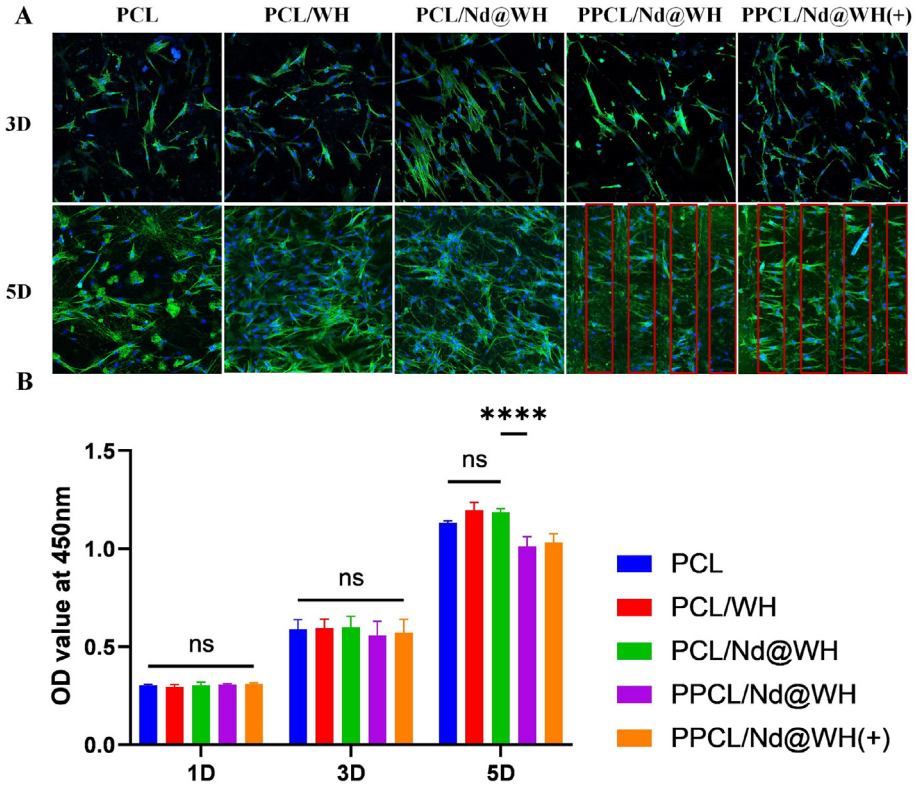

Fig. 5. Biocompatibility of different nanofiber membranes. (A) 3 and 5 days of BMSCs morphology. (B) CCK-8 determination of BMSCs proliferation after 1, 3, and 5 days (SD represents an intergroup error, ns represents no significant difference, ****p < 0.0001).

3.2. Evaluations of in vitro performance

3.2.1. In vitro biocompatibility

In this study, BMSCs were used to evaluate the effects of different nanofiber membranes on initial cell adhesion and proliferation. Fig. 5A shows that cells on different fibrous membranes do not show obvious inhibition over time. BMSCs proliferation was observed in different specimens. However, there was no significant difference in the cell compatibility between the pure PCL group and the other four groups within 1 and 3 days, indicating that WH and Nd@WH doping had no obvious cytotoxicity to BMSCs. At the same time, the comparison between PPCL/Nd@WH and PPCL/Nd@WH (+) groups at 1, 3, and 5 days showed that the application of external heating stimuli had no significant effect on cell activity. These structures suggest that surface micropatterning and photothermal stimulation have no significant effect on cell growth and proliferation (Fig. 5B). Compared with other control groups, the cells on PPCL/Nd@WH showed an obvious directional alignment trend. This provides an excellent surface structure for cell arrangement and angiogenesis.

3.2.2. Osteogenic differentiation

Many studies have shown that periosteal materials need excellent angiogenesis and bone-setting induction. Ca^{2+}, Mg^{2+}, and PO_4^{3-} *in vivo* can promote osteogenic differentiation and mineralization, and play a key role in the proliferation and differentiation of stem cells [29,30]. In preosteogenesis, Sirius red staining in Fig. 6A was used to evaluate the ability of each group to produce collagen fibers. By comparing the 7-day results to assess the effect of doping with Nd elements, we found that PCL/WH promoted collagen secretion better than PCL/Nd@WH. However, for the effect of surface alignment structure, the collagen secretion of PPCL/Nd@WH was slightly larger than that of PCL/Nd@WH. Finally, the effect of external photothermal stimulation on collagen fiber secretion was discussed. The results showed that the group with external photothermal stimulation was better than the group without stimulation. In addition, the results of the secretion of collagen fibers also showed a similar trend at 7 and 14 days (Fig. 6B). Further, at the late stage of osteogenesis, we used alizarin red staining to count the amount of calcium deposition secreted by each group of osteoblasts after maturation to evaluate the differences in the osteogenic properties of each group *in vitro* (Fig. 6C). The results of 14 days and 21 days showed that PCL/WH and PCL/Nd@WH had the same calcium deposition, and the results were not significantly different. In the meantime, the introduction of surface micropatterns did not significantly affect calcium deposition. However, when the temperature-induced by photothermal stimulation increased, the calcium deposition increased significantly, and the PPCL/Nd@WH (+) group had the highest calcium deposition (Fig. 6D).

Here, RT-PCR was used to detect the expression of osteogenic differentiation genes, such as collagen type I (COL I), osteocalcin (OCN),

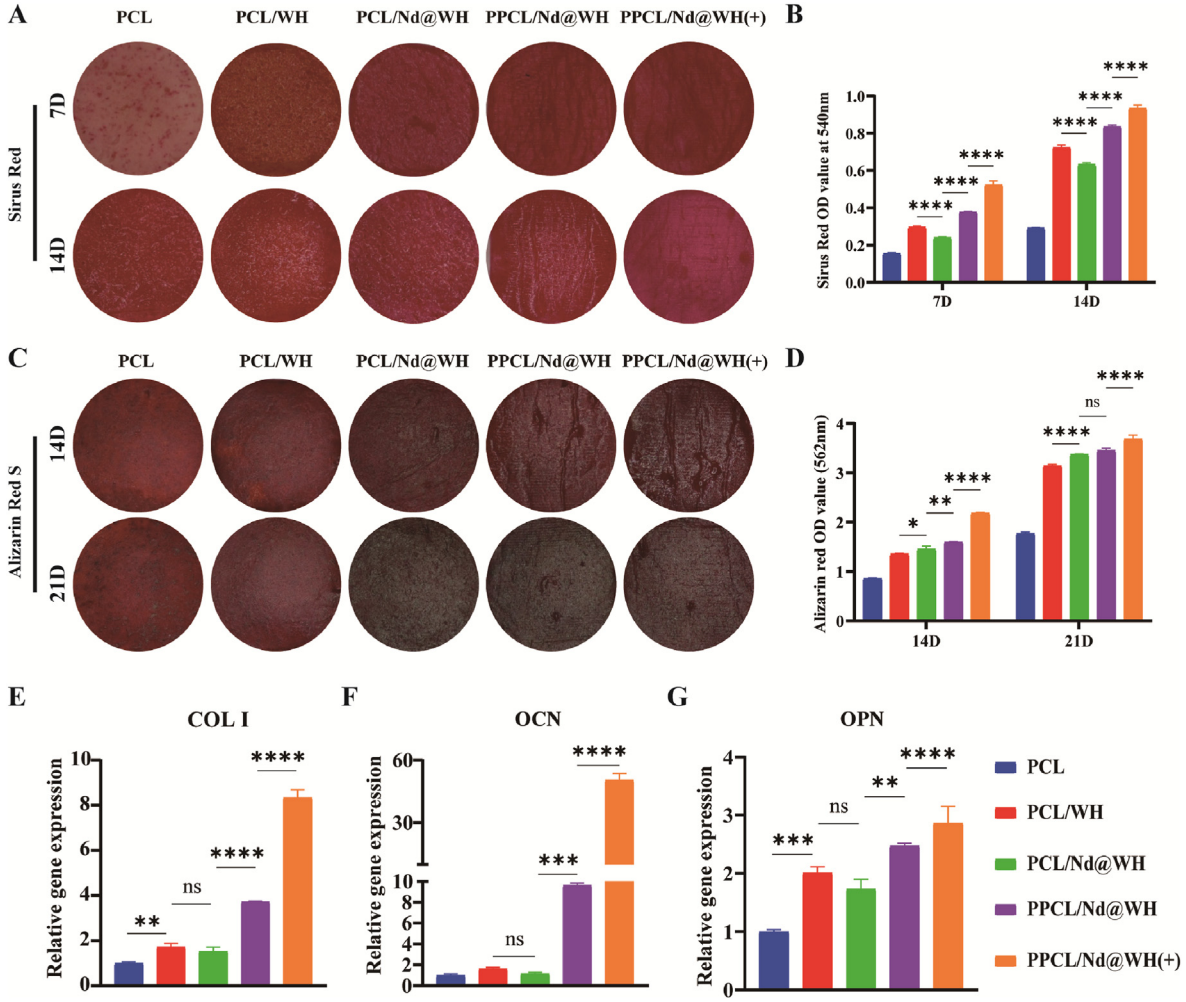

Fig. 6. Evaluation of osteogenic differentiation of cells in different membranes. (A) Sirius red staining qualitative analysis on days 7 and 14. (B) Sirius red quantitative analysis. (C) ARS qualitative analysis on days 14 and 21. (D) ARS quantitative analysis. The expression level of specific genes osteogenesis at 7 days (E) COL-I (F) OCN (G) OPN (SD represents an intergroup error, ns represents no significant difference, *p < 0.05 , **p < 0.01 , ***p < 0.001 , ****p < 0.0001).

and osteopontin (OPN), in BMSCs. From Fig. 6E and F, we can also see a similar trend that the PCL/WH and PCL/Nd@WH groups are similar in the amount of COL I and OCN secretion. However, when combining the surface-arranged structure with external photothermal stimulation, we found that the secretion of COL I and OCN was subsequently significantly increased. The results in Fig. 6G also suggest that the addition of surface-arranged structures and external photothermal stimulation have a synergistic effect on OPN secretion. Based on the above analysis, we can conclude that the application of the surface alignment structure in combination with external photothermal stimulation proved to be beneficial in regulating the osteogenic differentiation of BMSCs.

3.2.3. Neuroangiogenesis of PPCL/Nd@WH

We evaluated the effects of spun membranes on biocompatibility and neuroangiogenesis of neuronal cells and vascular endothelial cells, respectively.

As shown in Fig. 7A and B, there was no significant toxicity of the spun film to RAECs in each group, and also no significant inhibition of cell proliferation was seen. F-actin staining showed that the morphology of RAECs was not significantly affected (Fig. 7C). Here, RT-PCR was used to detect the expression of angiogenesis-related genes, such as CD31 (Fig. 7D) and eNOS (Fig. 7E). In terms of the expression of CD31 and eNOS, the PCL/WH, PCL/Nd@WH, PPCL/Nd@WH and PPCL/Nd@WH(+) groups all showed obviously higher expression than the PCL group, among which the PPCL/Nd@WH(+) group always had the highest expression. As for the cell migration experiment (Fig. 7F and H), PCL/WH, PCL/Nd@WH and PPCL/Nd@WH groups had better promoting migration effect to REACs compared with PCL group, and PCL/Nd@WH group was higher than PCL/WH group, but there was no significant difference between PCL/Nd@WH group and PPCL/Nd@WH group. Compared with other groups, the PPCL/Nd@WH(+) group had the best effect, indicating that photothermal treatment could promote the migration of RAECs. The above results indicated that the combined application of photothermal treatment and PPCL/Nd@WH was more favorable to promote neovascularization and the formation of periosteal vessels. A subcutaneous implantation experiment was used to verify the angiogenesis ability of each group. Five nanofibrous membranes were implanted between the skin and muscle of the SD rat's back. During the 14-day procedure, external photothermal stimulation was performed every other day at 0.5 W/cm^2 for 5 min. As shown in Figs. S8 and S9, the rat subcutaneous implantation experiment was stimulated and recorded temperature every 1 min. The results showed that after 1 min of interference, the defect material could be heated to about 40 °C. After 14 days, by H&E, Masson staining, and CD31 immunohistochemical staining (Fig. 7H), we could see the difference in angiogenic ability between the groups. The results showed that the angiogenesis ability of the PCL/WH group was higher than that of the PCL/Nd@WH group due to the high release of Mg^{2+}. The study found that when the surface of the material has an arranged structure, it can also promote angiogenesis. Therefore, the combined effect due to surface topography and ion release was considered. Therefore, PPCL/Nd@WH and PPCL/Nd@WH (+) had a significant angiogenic effect.

To verify the neurogenic activity of PPCL/Nd@WH, we co-cultured the nanofiber membranes with RSCs. After 1 and 3 days, CCK8 results showed that the membrane had not significantly cytotoxic to RSCs (Fig. 8A), and the live-dead staining showed that most of the cells were alive (green color) indicating that the spun films had good cytocompatibility for RSCs (Fig. 8B). Cell migration experiments of RSCs showed that both WH and Nd@WH-doped membranes had a significant promotion effect, and the PPCL/Nd@WH(+) group had the optimal effect, which indicated that photothermal treatment had a certain promotion effect on cell migration (Fig. 8C and D)and from the gene expression of NGF and S100 (Fig. 8E and F), both WH and Nd@WH could highly promote the expression of neural-related genes. The PPCL/Nd@WH(+) group also had the best pro-neural effect, which indicated that photothermal treatment combined with PPCL/Nd@WH could significantly promote neurovascularization and facilitate the neurovascular network reconstruction in the periosteum.

3.3. Evaluations in vivo performance

3.3.1. Evaluation of osteogenesis in vivo of calvarial defect model

As shown in Fig. S10A, the regeneration of periosteum and bone defect was demonstrated by the calvarial defect model of SD rats *in vivo*, and the periosteum was removed during the operation. During the 8-week procedure, external photothermal stimulation was performed every other day at 0.5 W/cm^2 for 5 min. As shown in Figs. S10B and S10C, the rat calvarial defect was stimulated and recorded every 1 min. The results showed that after 1 min of interference, the defect material could be heated to about 40 °C, and the temperature would remain at the target temperature of 40.5 ± 0.5 °C after 1 min.

To verify the neurovascularization function and photothermal of PPCL/Nd@WH, we implanted the material into the calvarial defect model of SD rats and performed NGF and CD31 immunofluorescence staining on the 7th day after implantation. Fig. 9A showed nuclear DAPI staining, NGF, and CD31 immunofluorescence staining results. In this study, the nerve repair effect was evaluated by the expression level of NGF protein, and angiogenesis was evaluated by the expression level of CD31. It was found that compared with other groups, the expression levels of NGF and CD31 in the pure PCL nanofiber membrane group were the lowest. The expression of NGF and CD31 in PCL/Nd@WH nanofibers was lower than that in PCL/WH nanofibers. The ICP results in Fig. 4F showed that the release amount of Mg^{2+} in PCL/WH was double that in PCL/Nd@WH, indicating that the release amount of ions was directly related to the expression level of proteins.

There is also evidence that surface micropatterns are directly related to angiogenesis, and surface-oriented structures can significantly increase the probability of angiogenesis. Therefore, CD31 expression in PPCL/Nd@WH and PPCL/Nd@WH (+) groups was higher than that in PCL/Nd@WH. Most importantly, the above results showed that the PPCL/Nd@WH (+) group showed the highest expression of NGF protein and CD31 under the combined action of photothermal, surface micropatterns, and ion release, that is, the production area of nerve fibers and vascular networks was the largest. (Fig. 9B and C). This result was significantly different from PCL. Combined with the above studies, it was found that angiogenesis in the rat subcutaneous angiogenesis model and rat calvarial defect model had the same trend.

After 8 weeks, microscopic CT and histological analysis were performed. Firstly, 3D reconstruction was conducted on the defect site. As shown in Fig. 10A, PPCL/Nd@WH (+) has a significantly better repair effect, indicating the synergistic effect of ion release and photothermal stimulation on promoting osteogenesis. Compared with the pure PCL material control group, WH and Nd@WH nanofiber membranes have better osteogenic properties. This is because WH and Nd@WH can release Ca^{2+}, PO_4^{3-} ions to further promote osteogenesis. Subsequently, we further investigated the 3D reconstruction by analyzing the bone volume fraction. In the analysis of bone volume fraction, the value of the PPCL/Nd@WH (+) group was 2.5 times that of the PCL material control group (Fig. 10B). The bone volume fractions of PCL/WH, PCL/Nd@WH, and PPCL/Nd@WH were 36.65%, 41.61%, and 54.65%, respectively. Importantly, these results are consistent with the trend of microscopic CT.

Histological examination was investigated to further verify the microscopic details of the defect area. Before analysis, the defective and adjacent sites of material, new bone, and host bone were distinguished and labeled in the low field of view. As shown in H&E and Masson trichrome staining images (Fig. 10C), compared with other groups, PPCL/Nd@WH (+) coated defect areas formed more osteogenic arrays. At 8-week, a red color could be observed in Masson staining, which indicated the formation of regular lamellar bone in the bone tissue. Furthermore, Masson staining also showed that the PPCL/Nd@WH (+) group had more pronounced and continuous collagen matrix deposition

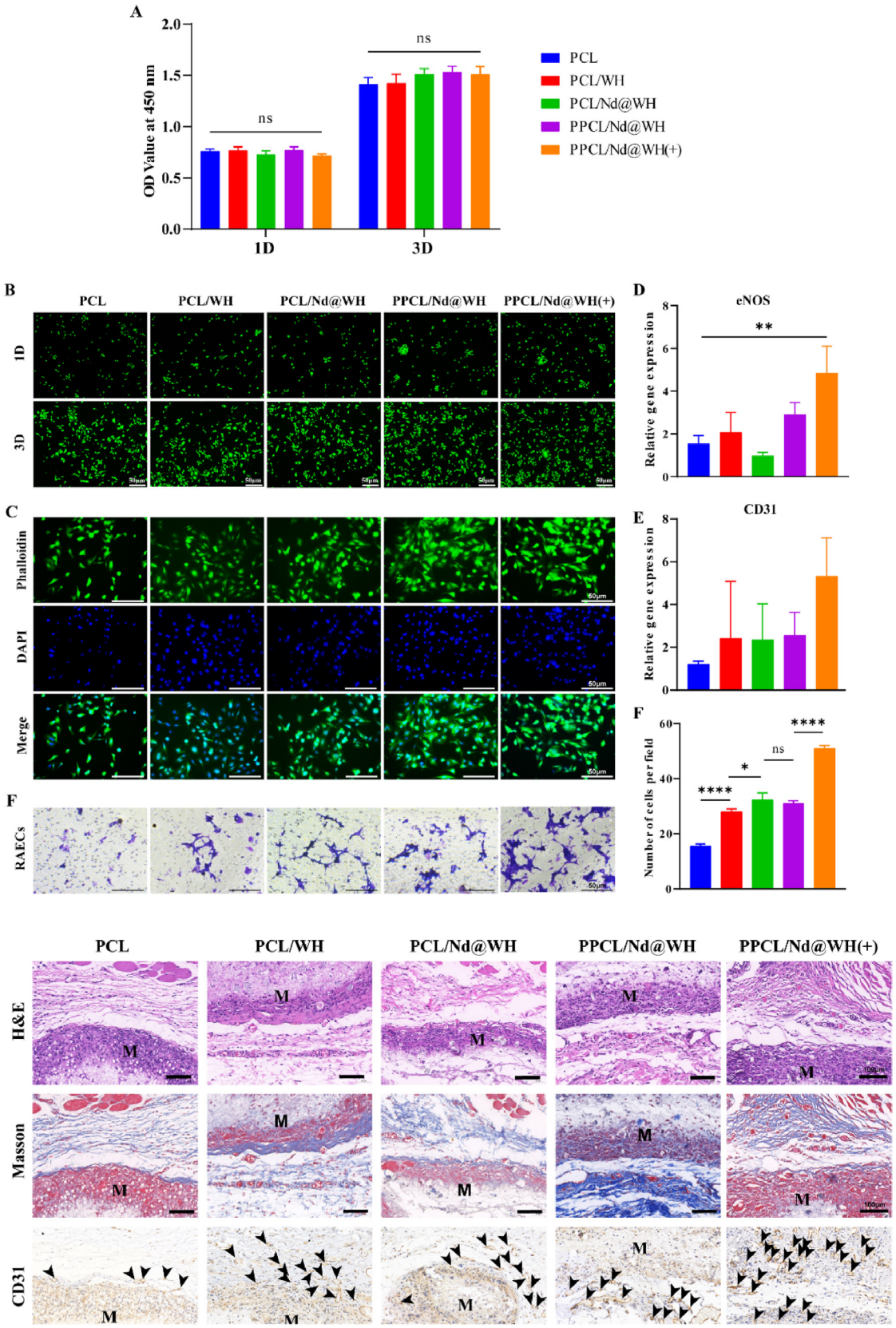

Fig. 7. Evaluation of angiogenesis of RAECs with different membranes. CCK-8 assay (A) and Live/dead assay of RAECs (B). (C) The morphology of RAECs cell. (D) The relative gene expression of RAECs cultured directly on different membranes at 1 day about eNOS (D) and CD31 (E). The representative images (F) and quantitative results (G) of transwell assay of RAECs cultured with different membranes. H&E, Masson, and CD31 histological images of different nanofiber membranes in subcutaneous model validation (Black arrows represent blood vessels, ns represents no significant difference, *p < 0.05 , **p < 0.01 , ***p < 0.001 , ****p < 0.0001).

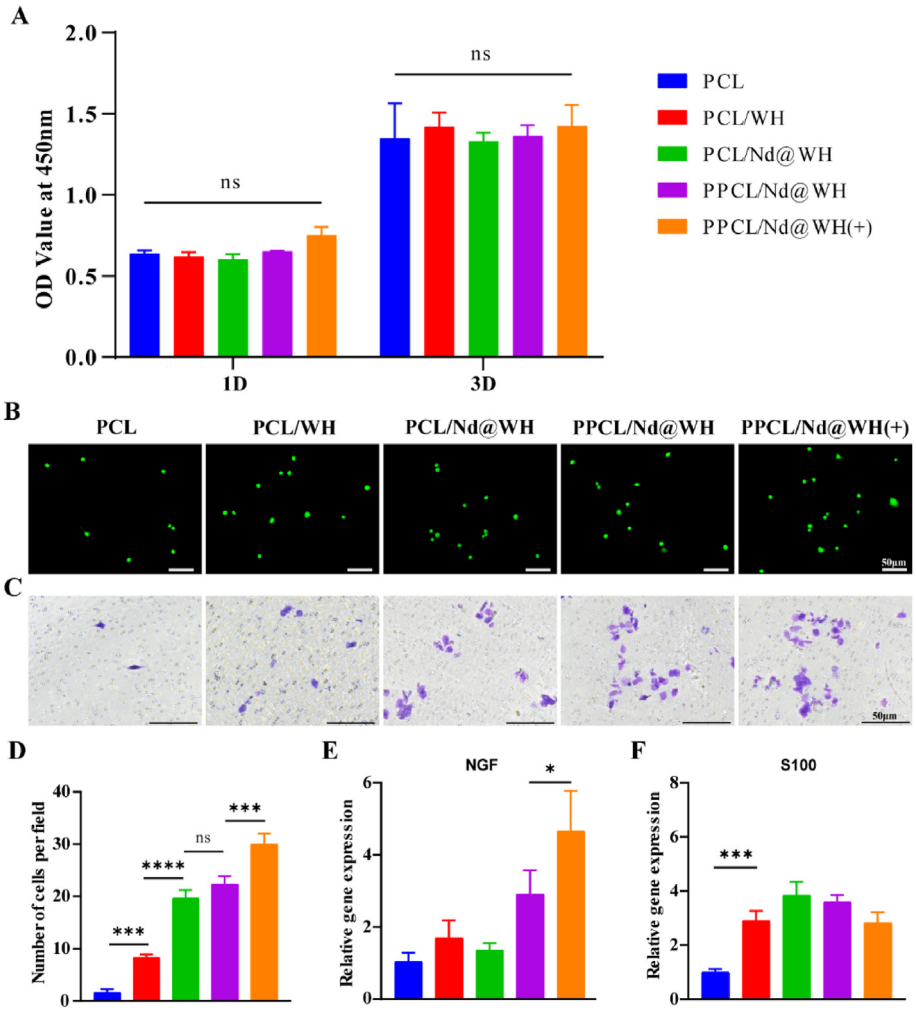

Fig. 8. Evaluation of angiogenesis of RAECs with different membranes. CCK-8 assay (A) and Live/dead assay of RSCs (B). The representative images (C) and quantitative results (D) of transwell assay of RAECs cultured with different membranes. The relative gene expression of RSCs cultured directly on different membranes at 1 day about NGF (E) and S100 (F). (ns represents no significant difference, *p < 0.05 , **p < 0.01 , ***p < 0.001 , ****p < 0.0001).

compared to the other groups. And compared to the material control group (PCL group), bone formation was higher in the other material groups, which are our expected results. At the same time, OCN (osteogenic marker) immunohistochemical staining also showed that PPCL/Nd@WH (+) can promote bone formation (Fig. S10), which is consistent with the results of microscopic CT and Masson staining.

The regeneration of periosteum and bone was verified in animal experiments. It is well known that regeneration is a complex process. The co-staining of NGF and VEGF proved that nerve and blood vessels were accompanied by growth in endogenous periosteal regeneration. On the other hand, the results of *in vitro* cell proliferation experiment showed that the cells had the tendency of oriented growth on the electrospinning membrane. This demonstrates that the periosteum can help achieve simultaneously regeneration in structure and function. And the combination of ionic action and photothermal osteogenesis can further promote bone formation and ultimately achieve bone regeneration.

As is well-known to all, the periosteum is a highly complex structure. Thus, to achieve all its functions, it lacks practical feasibility as far as it is concerned. Consequently, there is still a gap between the bionic periosteum and the natural periosteum, and further improvements are still needed.

4. Discussion

Compared with the current popular periosteal reconstruction methods, inspired by the structure and function of natural periosteum, the spinning template with a surface-oriented structure was prepared by laser etching technology. The template was fixed on the collector, and the photothermal double-layer bionic periosteum with nerve-vascular coupling regeneration was prepared by electrospinning technology.

The periosteum is a double connective tissue membrane with rich cell sources [1,15]. In this study, a double-layer biomimetic periosteum was constructed by imitating the double-layer structure of natural periosteum. The outer layer of the bionic periosteum not only provides early barrier function but also avoids soft tissue invasion into bone defects [31–34]. The repair of bone defects was also accelerated through neurovascular reconstruction, cell recruitment, and bone regeneration. The inner layer of the bionic periosteum promotes the regeneration of nerve vessels and bones through topological clues of surface topography [5,35]. Firstly, structural bionics is realized. the surface-oriented micropatterns of PPCL/Nd@WH were successfully constructed by SEM, while the PCL/Nd@WH group without surface-oriented micropatterns showed the surface morphology of the conventional electrospinning membrane. The

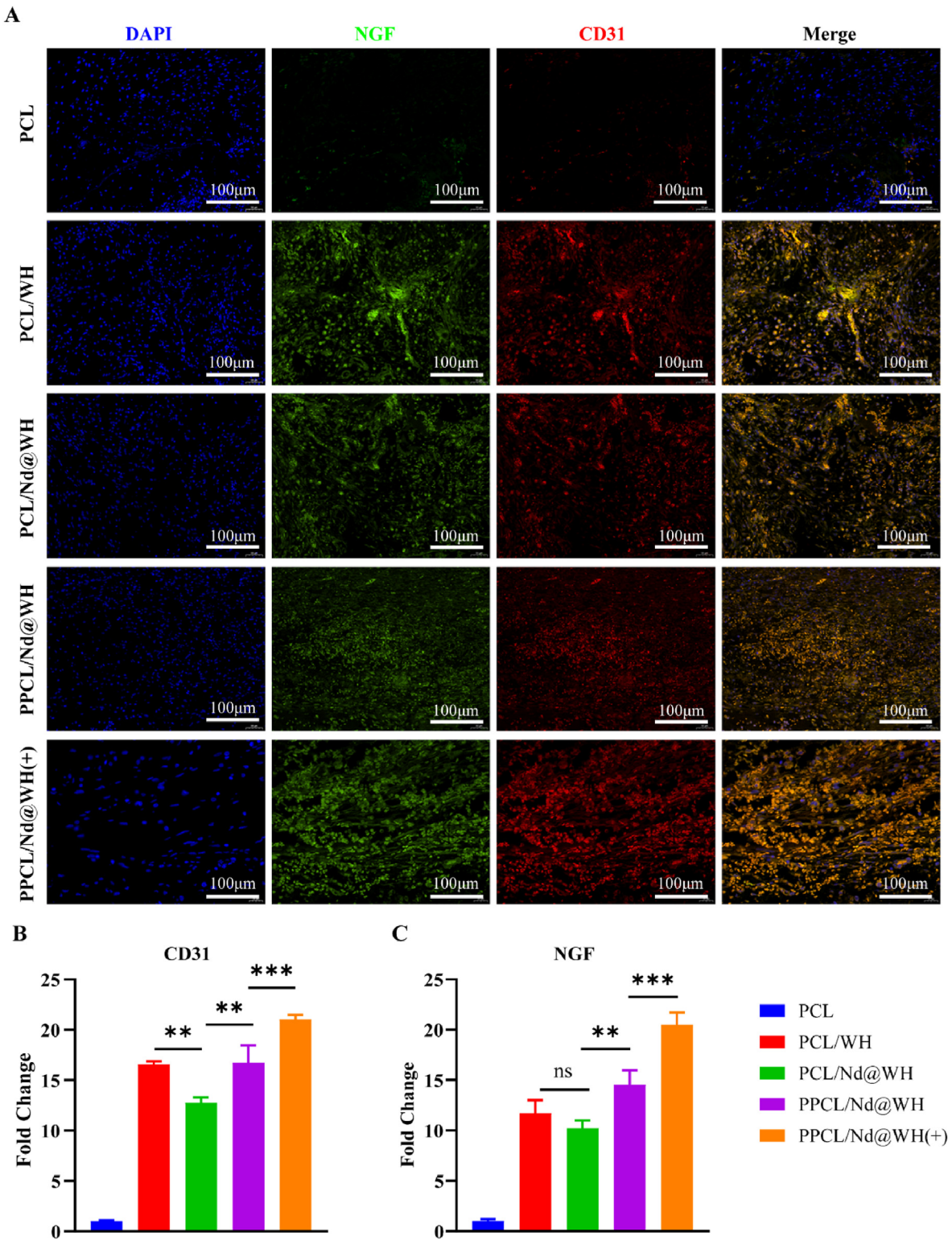

Fig. 9. (A) Expression node of neurovascularization in rat calvarial defect experiment. (B) 7 days after implantation, each material group showed different fluorescence intensity. Quantitative analysis of (C) CD31 and (D) NGF. (ns represents no significant difference, *p < 0.05 , **p < 0.01 , ***p < 0.001 , ****p < 0.0001).

SEM results showed that the bi-layer biomimetic periosteum with different functions was successfully prepared in this study (Fig. 2). Through cell proliferation experiment, PPCL/Nd@WH group with surface-oriented micropatterns can observe the orientation arrangement of cells (Fig. 5). By testing the secretion of collagen fibers, the deposition of calcium nodules, and the expression of osteogenic-related genes, it can be intuitively seen from the data that the expression of PPCL/Nd@WH small-component bone in the patterned group was significantly higher than that in the PCL/Nd@WH group without patterning (Fig. 6). Finally, the angiogenesis ability and osteogenic ability of the PPCL/Nd@WH group were compared with PCL/Nd@WH group in the subcutaneous angiogenesis experiment and rat skull defect model (Figs. S8–10).

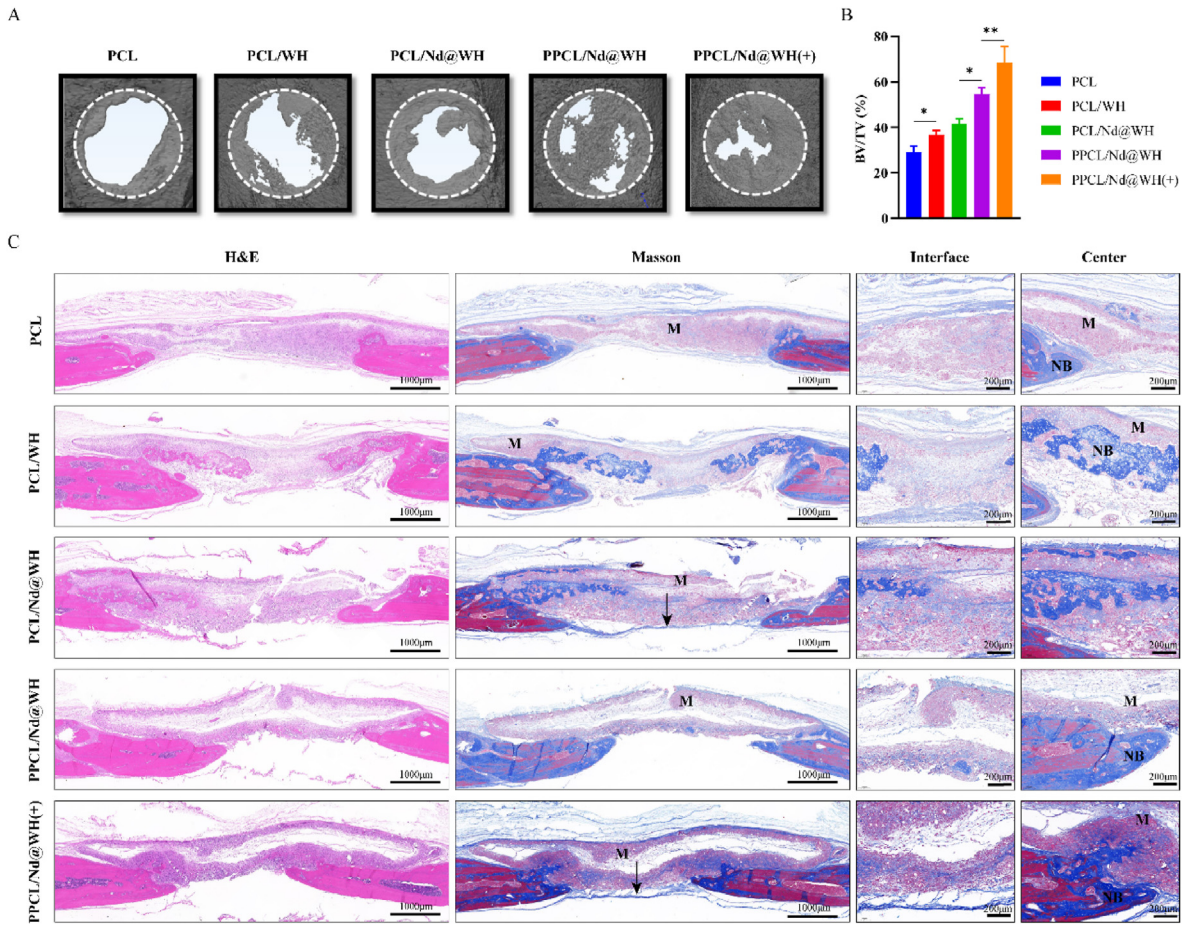

Fig. 10. Analysis of osteogenic properties of different nanofiber membranes. (A) 3D reconstruction images of the defect area. (B) volume fraction of bone (BV/TV) (SD represents intergroup error, *p < 0.05 , **p < 0.01). (C) histological analysis of H&E and Masson staining (black arrows for continuous collagen fibers, M for materials, NB for newly formed bone).

Periosteum has three functions. First, the periosteum has abundant cell sources; secondly, the periosteum can also provide necessary growth factors to regulate bone homeostasis; third, under the stimulation of external mechanical force, periosteal-derived cells respond quickly and can activate Wnt and BMP signaling pathways to promoting bone formation [15,36–39]. So the functional bionics of the periosteum should be valued [14]. Based on WH, we doped characteristic photothermal response Nd element in WH by hydrothermal synthesis method, and finally endowed WH with photothermal response performance, namely Nd@WH. The functional ions of WH and Nd@WH were similar, and the ion release in different biomimetic periosteums was measured by inductively coupled plasma emission spectrometry (Fig. 3F). The results showed that Ca^{2+}, Mg^{2+}, and PO_4^{3-} were released from PCL/Nd@WH and PCL/WH. It is well known that Ca^{2+} and PO_4^{3-} are necessary inorganic ions in the process of bone formation, which are involved in bone remodeling. On this basis, the cell biocompatibility and osteogenic differentiation ability of PCL/WH and PCL/Nd@WH were tested, and it was found that the cell biocompatibility of PCL\WH and PCL/Nd@WH had no significant influence (Fig. 5), but the osteogenic differentiation ability of PCL\WH was significantly higher than that of PCL/Nd@WH (Fig. 6). In addition, Mg^{2+} is a potential active factor in promoting neurovascularization. studies have shown that sustained release of Mg^{2+} can effectively promote the release of VEGF. Therefore, *in vitro* experiments verified that it can significantly promote angiogenesis (Fig. 7), and at the same time through the verification of the rat subcutaneous angiogenesis model and skull defect model, it was observed that the angiogenesis effect of PCL/WH and PCL/Nd@WH groups was good (Fig. S11). At the same time, some literature showed that the continuous release of Mg^{2+} could effectively promote the release of NGF. Therefore, in the rat skull defect model, the immunofluorescence staining intensity of NGF and CD31 was used to express the regeneration of nerve and blood vessels in the defect area. The results showed that compared with other groups, the fluorescence intensity of PCL/WH and PCL/Nd@WH groups were higher, indicating that their neurovascularization effect was good (Figs. 7–9).

Some studies have shown that elevated temperature in the fracture site is closely related to new bone formation. Heat above the body temperature of about 3 °C can stimulate animal bone growth [28,40,41]. So we can point out that when the temperature is about 40 °C, the temperature will stimulate bone regeneration in the defect site. In this study, the Nd element was stimulated by near-infrared light to generate heat, thereby promoting bone regeneration. Firstly, the photothermal response of PPCL/Nd@WH was verified by photothermal response performance. The results showed that the PPCL/Nd@WH bionic periosteum had good photothermal response characteristics under 808 nm wavelength near-infrared irradiation, and this bionic periosteum could rapidly rise to about 40 °C in 60 s (Fig. 3E). A large number of kinds of literature proved that the bone regeneration of the defect site was significantly improved under this temperature. Compared with PPCL/Nd@WH , the PPCL/Nd@WH(+) group showed an excellent osteogenic differentiation effect was subjected to external near-infrared physical stimulation. In particular, this study found that the external near-infrared stimulation group PPCL/Nd@WH(+), the neurovascular effect is obvious. However, its mechanism remains unclear and needs further study.

Therefore, through the double bionics of structure and function, the

double bionic periosteum with good interlayer binding force was constructed by integrated molding. The good flexibility and operability of the PPCL/Nd@WH bionic periosteum were verified by tensile properties (Fig. 3B). PPCL/Nd@WH biomimetic periosteum can effectively repair the defect site of rat skull model under the common stimulation of surface orientation micropattern, photothermal effect, and ion effect.

5. Conclusion

In summary, inspired by the structure and function of the periosteum, we successfully developed a neurovascularized double-layer nanofiber membrane as a biomimetic periosteum. Through the release of Mg^{2+} ions from Nd@WH nanoparticles in nanofiber membrane with surface alignment structure, the formation of endogenous periosteum was induced and the regeneration of internal and external source composite periosteum was realized. The regeneration of the periosteum was further confirmed by the detection of increased secretion of VEGF and NGF factors. This was necessary for nerve and vascular growth to demonstrate the simultaneous growth of nerves and blood vessels. Combined with surface micropatterning, electrospinning, and photothermal bone formation, the periosteum can accelerate bone formation. Therefore, in this study, a double-layer nanofiber membrane as biomimetic periosteum may bring great hope for the clinical treatment of secondary surgery caused by a bone defect or nonunion.

Credit author statement

Qing Li: Conceptualization, Methodology, Formal analysis, Investigation, Data curation, Writing – original draft, Visualization. **Wenbin Liu**: Conceptualization, Methodology, Formal analysis, Investigation, Data curation, Writing – original draft, Visualization, Funding acquisition. **Wen Hou**: Investigation, Data curation. **Xiaopei Wu**: Investigation. **Wenying Wei**: Investigation. **Jiawei Liu**: Investigation. **Yihe Hu**: Writing – review & editing, Supervision. **Honglian Dai**; Conceptualization, Writing – review & editing, Supervision, Project administration, Funding acquisition.

Declaration of competing interest

The authors declare that they have no known competing financial interests or personal relationships that could have appeared to influence the work reported in this paper.

Data availability

Data will be made available on request.

Acknowledgments

This work was supported by grants from the National Natural Science Foundation of China (51772233, and 32201109), the Guangdong Basic and Applied Basic Research Foundation (2022B1515120052, 2021A1515110557), the Key Basic Research Program of Shenzhen (JCYJ20200109150218836), and the project supported by State Key Laboratory of Advanced Technology for Materials Synthesis and Processing (2022-KF-8).

Appendix A. Supplementary data

Supplementary data to this article can be found online at https://doi.org/10.1016/j.mtbio.2022.100536.

References

[1] E. Seeman, The periosteum—a surface for all seasons, Osteoporos. Int. 18 (2007) 123–128.
[2] P. Carmeliet, M. Tessier-Lavigne, Common mechanisms of nerve and blood vessel wiring, Nature 436 (7048) (2005) 193–200.
[3] X. Lin, S. Patil, Y.-G. Gao, A. Qian, The bone extracellular matrix in bone formation and regeneration, Front. Pharmacol. 11 (2020) 757.
[4] X. Dong, P. Wu, L. Yan, K. Liu, W. Wei, Q. Cheng, X. Liang, Y. Chen, H. Dai, Oriented nanofibrous P (MMD-co-LA)/Deferoxamine nerve scaffold facilitates peripheral nerve regeneration by regulating macrophage phenotype and revascularization, Biomaterials 280 (2022), 121288.
[5] L. Fan, J.-L. Li, Z. Cai, X. Wang, Creating biomimetic anisotropic architectures with co-aligned nanofibers and macrochannels by manipulating ice crystallization, ACS Nano 12 (6) (2018) 5780–5790.
[6] Y. Zhao, Y. Liang, S. Ding, K. Zhang, H.-q. Mao, Y. Yang, Application of conductive PPy/SF composite scaffold and electrical stimulation for neural tissue engineering, Biomaterials 255 (2020), 120164.
[7] W. Jiang, L. Li, D. Zhang, S. Huang, Z. Jing, Y. Wu, Z. Zhao, L. Zhao, S. Zhou, Incorporation of aligned PCL–PEG nanofibers into porous chitosan scaffolds improved the orientation of collagen fibers in regenerated periodontium, Acta Biomater. 25 (2015) 240–252.
[8] J. Xue, J. Xie, W. Liu, Y. Xia, Electrospun nanofibers: new concepts, materials, and applications, Acc. Chem. Res. 50 (8) (2017) 1976–1987.
[9] Y. Jia, W. Yang, K. Zhang, S. Qiu, J. Xu, C. Wang, Y. Chai, Nanofiber arrangement regulates peripheral nerve regeneration through differential modulation of macrophage phenotypes, Acta Biomater. 83 (2019) 291–301.
[10] X. Dong, S. Liu, Y. Yang, S. Gao, W. Li, J. Cao, Y. Wan, Z. Huang, G. Fan, Q. Chen, Aligned microfiber-induced macrophage polarization to guide schwann-cell-enabled peripheral nerve regeneration, Biomaterials 272 (2021), 120767.
[11] G. Yang, H. Liu, Y. Cui, J. Li, X. Zhou, N. Wang, F. Wu, Y. Li, Y. Liu, X. Jiang, Bioinspired membrane provides periosteum-mimetic microenvironment for accelerating vascularized bone regeneration, Biomaterials 268 (2021), 120561.
[12] G. Abagnale, M. Steger, V.H. Nguyen, N. Hersch, A. Sechi, S. Joussen, B. Denecke, R. Merkel, B. Hoffmann, A. Dreser, Surface topography enhances differentiation of mesenchymal stem cells towards osteogenic and adipogenic lineages, Biomaterials 61 (2015) 316–326.
[13] Q. Wang, J. Xu, H. Jin, W. Zheng, X. Zhang, Y. Huang, Z. Qian, Artificial periosteum in bone defect repair—a review, Chin. Chem. Lett. 28 (9) (2017) 1801–1807.
[14] H. Chang, M.L. Knothe Tate, Concise review: the periosteum: tapping into a reservoir of clinically useful progenitor cells, Stem Cells Trans. Med. 1 (6) (2012) 480–491.
[15] W. Zhang, N. Wang, M. Yang, T. Sun, J. Zhang, Y. Zhao, N. Huo, Z. Li, Periosteum and development of the tissue-engineered periosteum for guided bone regeneration, J. Orthop. Trans. 33 (2022) 41–54.
[16] R.F. Bombaldi de Souza, Â.M. Moraes, Hybrid bilayered chitosan-xanthan/PCL scaffolds as artificial periosteum substitutes for bone tissue regeneration, J. Mater. Sci. (2022) 1–17.
[17] C. Dong, F. Qiao, G. Chen, Y. Lv, Demineralized and decellularized bone extracellular matrix-incorporated electrospun nanofibrous scaffold for bone regeneration, J. Mater. Chem. B 9 (34) (2021) 6881–6894.
[18] R.C. Gresham, C.S. Bahney, J.K. Leach, Growth factor delivery using extracellular matrix-mimicking substrates for musculoskeletal tissue engineering and repair, Bioact. Mater. 6 (7) (2021) 1945–1956.
[19] Y. Yang, T. Xu, Q. Zhang, Y. Piao, H.P. Bei, X. Zhao, Biomimetic, stiff, and adhesive periosteum with osteogenic–angiogenic coupling effect for bone regeneration, Small 17 (14) (2021), 2006598.
[20] H.D. Kim, H.L. Jang, H.-Y. Ahn, H.K. Lee, J. Park, E.-s. Lee, E.A. Lee, Y.-H. Jeong, D.-G. Kim, K.T. Nam, Biomimetic whitlockite inorganic nanoparticles-mediated in situ remodeling and rapid bone regeneration, Biomaterials 112 (2017) 31–43.
[21] H.L. Jang, K. Jin, J. Lee, Y. Kim, S.H. Nahm, K.S. Hong, K.T. Nam, Revisiting whitlockite, the second most abundant biomineral in bone: nanocrystal synthesis in physiologically relevant conditions and biocompatibility evaluation, ACS Nano 8 (1) (2014) 634–641.
[22] J. Mi, J. Xu, H. Yao, X. Li, W. Tong, Y. Li, B. Dai, X. He, D.H.K. Chow, G. Li, Calcitonin gene-related peptide enhances distraction osteogenesis by increasing angiogenesis, Tissue Eng. 27 (1–2) (2021) 87–102.
[23] L. Sun, M. Wang, S. Chen, B. Sun, Y. Guo, C. He, X. Mo, B. Zhu, Z. You, Molecularly engineered metal-based bioactive soft materials–neuroactive magnesium ion/polymer hybrids, Acta Biomater. 85 (2019) 310–319.
[24] Y. Zhang, J. Xu, Y.C. Ruan, M.K. Yu, M. O'Laughlin, H. Wise, D. Chen, L. Tian, D. Shi, J. Wang, Implant-derived magnesium induces local neuronal production of CGRP to improve bone-fracture healing in rats, Nat. Med. 22 (10) (2016) 1160–1169.
[25] J. Li, A. Kreicbergs, J. Bergström, A. Stark, M. Ahmed, Site-specific CGRP innervation coincides with bone formation during fracture healing and modeling: a study in rat angulated tibia, J. Orthop. Res. 25 (9) (2007) 1204–1212.
[26] K. Ma, C. Liao, L. Huang, R. Liang, J. Zhao, L. Zheng, W. Su, Electrospun PCL/MoS2 nanofiber membranes combined with NIR-triggered photothermal therapy to accelerate bone regeneration, Small 17 (51) (2021), 2104747.
[27] L. Tong, Q. Liao, Y. Zhao, H. Huang, A. Gao, W. Zhang, X. Gao, W. Wei, M. Guan, P.K. Chu, Near-infrared light control of bone regeneration with biodegradable photothermal osteoimplant, Biomaterials 193 (2019) 1–11.
[28] J. Chen, Z.-D. Shi, X. Ji, J. Morales, J. Zhang, N. Kaur, S. Wang, Enhanced osteogenesis of human mesenchymal stem cells by periodic heat shock in self-assembling peptide hydrogel, Tissue Eng. 19 (5–6) (2013) 716–728.
[29] G.R. Beck, B. Zerler, E. Moran, Phosphate is a specific signal for induction of osteopontin gene expression, Proc. Natl. Acad. Sci. USA 97 (15) (2000) 8352–8357.
[30] G.R. Beck Jr., Inorganic phosphate as a signaling molecule in osteoblast differentiation, J. Cell. Biochem. 90 (2) (2003) 234–243.

[31] Y. He, Y. Tian, W. Zhang, X. Wang, X. Yang, B. Li, L. Ge, D. Bai, D. Li, Fabrication of oxidized sodium alginate-collagen heterogeneous bilayer barrier membrane with osteogenesis-promoting ability, Int. J. Biol. Macromol. 202 (2022) 55–67.
[32] Y. Qian, X. Zhou, F. Zhang, T.G. Diekwisch, X. Luan, J. Yang, Triple PLGA/PCL scaffold modification including silver impregnation, collagen coating, and electrospinning significantly improve biocompatibility, antimicrobial, and osteogenic properties for orofacial tissue regeneration, ACS Appl. Mater. Interfaces 11 (41) (2019) 37381–37396.
[33] M. Gong, C. Chi, J. Ye, M. Liao, W. Xie, C. Wu, R. Shi, L. Zhang, Icariin-loaded electrospun PCL/gelatin nanofiber membrane as potential artificial periosteum, Colloids Surf. B Biointerfaces 170 (2018) 201–209.
[34] M. Gong, C. Huang, Y. Huang, G. Li, C. Chi, J. Ye, W. Xie, R. Shi, L. Zhang, Core-sheath micro/nano fiber membrane with antibacterial and osteogenic dual functions as biomimetic artificial periosteum for bone regeneration applications, Nanomed. Nanotechnol. Biol. Med. 17 (2019) 124–136.
[35] D. Zhang, Y. Yao, Y. Duan, X. Yu, H. Shi, J.R. Nakkala, X. Zuo, L. Hong, Z. Mao, C. Gao, Surface-anchored graphene oxide nanosheets on cell-scale micropatterned poly (d, l-lactide-co-caprolactone) conduits promote peripheral nerve regeneration, ACS Appl. Mater. Interfaces 12 (7) (2020) 7915–7930.
[36] R. Ito, T. Matsumiya, T. Kon, N. Narita, K. Kubota, H. Sakaki, T. Ozaki, T. Imaizumi, W. Kobayashi, H. Kimura, Periosteum-derived cells respond to mechanical stretch and activate Wnt andBMP signaling pathways, Biomed. Res. 35 (1) (2014) 69–79.
[37] M. Rozis, V. Polyzois, S. Pneumaticos, The distraction osteogenesis callus: a review of the literature, Clin. Rev. Bone Miner. Metabol. 19 (2022) 24–35.
[38] S. Debnath, A.R. Yallowitz, J. McCormick, S. Lalani, T. Zhang, R. Xu, N. Li, Y. Liu, Y.S. Yang, M. Eiseman, Discovery of a periosteal stem cell mediating intramembranous bone formation, Nature 562 (7725) (2018) 133–139.
[39] S. Méndez-Ferrer, T.V. Michurina, F. Ferraro, A.R. Mazloom, B.D. MacArthur, S.A. Lira, D.T. Scadden, A. Ma'ayan, G.N. Enikolopov, P.S. Frenette, Mesenchymal and haematopoietic stem cells form a unique bone marrow niche, Nature 466 (7308) (2010) 829–834.
[40] J.R. Doyle, B.W. Smart, Stimulation of bone growth by short-wave diathermy, J. Bone Joint Surg. 45 (1) (1963) 15–24.
[41] V. Richards, R. Stofer, The stimulation of bone growth by internal heating, Soc. Univ. Surg. 46 (1) (1959) 84–96.